Systematic approach to the development of microfabricated biosensors: relationship between the gold surface pretreatment and thiolated molecule binding

Asta Makaraviciute[1], *Xingxing Xu*[1], *Leif Nyholm*[2], *Zhen Zhang*[1*]

AUTHOR ADDRESS

[1]Division of Solid-State Electronics, Department of Engineering Sciences, The Ångström Laboratory, Uppsala University, P.O. Box 534, SE-751 21 Uppsala, Sweden

[2]Department of Chemistry, The Ångström Laboratory, Uppsala University, P.O. Box 534, SE-751 21 Uppsala, Sweden

*Corresponding author: Zhen.Zhang@angstrom.uu.se

KEYWORDS

Surface pretreatment, surface characterization, surface functionalization, gold, mercaptohexanol, cyclic voltammetry, XPS, biosensor, microfabrication

ABSTRACT

Despite increasing popularity of microfabricated biosensors due to advances in technologic and surface functionalization strategies, their successful implementation is partially inhibited by the lack of consistency in their analytical characteristics. One of the main causes for the discrepancies is the absence of a systematic and comprehensive approach to surface functionalization. In this contribution microfabricated gold electrodes aimed at biosensor development have been systematically characterized in terms of surface pretreatment, thiolated molecule binding and reproducibility by the means of X-ray photoelectron scattering (XPS) and cyclic voltammetry (CV). It has been shown that after SU-8 photolithography gold surfaces were markedly contaminated, which decreased the effective surface area and surface coverage of a model molecule mercaptohexanol (MCH). Three surface pretreatment methods compatible with microfabricated devices were compared. The investigated methods were (i) cyclic voltammetry in dilute H_2SO_4, (ii) gentle basic piranha followed by linear sweep voltammetry in dilute KOH and (iii) oxygen plasma treatment followed by incubation in ethanol. It was shown that all three methods significantly decreased the contamination and increased MCH surface coverage. Most importantly, it was also revealed that surface pretreatments may induce structural changes to the gold surfaces. Accordingly, these alterations influence the characteristics of MCH functionalization.

INTRODUCTION

Miniaturization and multiplex sensing have become leading directions in the development of new generation biosensors.[1,2] However, for successful practical implementation it is highly desirable that biosensors meet a set of validation requirements, such as, high selectivity, sensitivity, reproducibility, stability, low sample volumes and user-friendly operation.[3] One way of addressing the posed challenges is the use of silicon microfabrication technology, which enables fabrication of ultrasensitive nanoscale devices with rapid responses, low prices, large scale production and integration with microfluidic systems.

Among the different examples of silicon technology-based biosensors, ion-sensitive field-effect transistors (ISFETs) have been particularly successfully applied[4,5], especially for label-less DNA sensing and sequencing.[6,7] The sensing principle of a ISFET is based on adsorption of charged species on the sensor surface, which leads to a change in surface potential and hence a change in current in the ISFET channel. Since DNA molecules are negatively charged, DNA hybridization with surface-bound probes can be registered by ISFET devices. However, despite the well-developed fabrication process and many innovative sensing strategies, ISFET sensitivities and other analytical characteristics vary to a great extent. This prevents their successful implementation in real sample analysis, validation and eventual commercialization. One of the reasons for such discrepancies in microfabricated biosensor development is the lack of control in surface modification. In particular, some technical difficulties requiring better solutions are: surface contamination, immobilization of biomolecules to avoid contamination, deeper understanding of the behavior of adsorbed molecules and uniformity of biomolecule preparation.[8]

When ISFETs are used for direct DNA sensing, thiolated DNA probes are often immobilized on gold-coated surfaces by spontaneously forming gold-thiol bonds. Thiol groups are affixed to DNA molecules by six carbon atom alkyl linkers.[9,10] In the case when no gold passivation is used, in addition to the gold-thiol bond each DNA probe forms multiple interactions between the amine groups of DNA nucleotides and gold.[11,12] As a result, DNA molecules adopt procumbent surface configuration. For this reason and in order to minimize the non-specific adsorption, the surface is often passivated by a self-assembled monolayer (SAM) of a thiolated alcohol mercaptohexanol (MCH), which is of the same length as the alkyl linkers of DNA probes. This way gold-amine interactions are displaced by gold-thiol bonds and, as a

result, DNA probes take rod-like configuration.[13,14] Moreover, due to compatible dimensions of MCH molecules and DNA linkers, probes are not blocked by the passivating molecules. However, it is important to keep in mind that since gold-thiolate bonding is a dynamic system, DNA probes are partly replaced by MCH in this process. Furthermore, some DNA probes are also lost during the sensor operation or storage.[15,16] Finally, due to this deceivingly simple approach to surface functionalization, its critical aspects, such as gold surface preparation and evaluation of DNA probe immobilization efficiency, as well as their reproducibility, are often dismissed, although it has been long known that these parameters directly affect biosensor characteristics.[8,13,17]

What is more, it has been shown that photolithography used in microfabrication of silicon devices may result in contamination.[18,19] In the case of gold-coated surfaces, the contamination issue is often believed to be circumvented by surface cleaning. However, the cleaning is often done by oxidizing surface pretreatments, such as UV plasma or piranha solution despite the fact that damaging consequences of such treatments have been reported. For example, piranha treatment may produce oxidized sulfur near-surface region, which, in turn, results in a decrease of binding sites for thiol-modified molecules.[20] In another instance, it has been shown that UV plasma treatment induces structural surface changes, as observed by STM.[21] Moreover, the efficiency of cleaning methods is usually not addressed either. Knowing what surface area is available for binding enables to obtain optimal molecule surface density, which leads to controlled sensitivity and reproducibility. Unsurprisingly, problems related to gold functionalization by the thiolated molecules have been reported. For example, it has been shown that immobilized DNA molecules are lost from the sensor surface during storage[16] or form aggregates.[22]

For these reasons in this study gold electrode surfaces patterned with SU-8 photolithography have been investigated. SU-8 is commonly employed to passivate micro-electrode arrays and to define active area in ISFET fabrication.[23,24] Its main advantages are low temperature and low-cost processes, which result in good passivation characteristics, such as high aspect ratio, dielectric strength, chemical resistance, mechanical properties and biocompatibility.[25,26] However, it has been reported that the use of photoresist results in contamination of the microfabricated structures.[18,19] Moreover, photoresist exhibits good adhesion on gold.[27] Nevertheless, the effects of its contamination and removal have not been systematically studied.

With an aim to avoid damage to the microfabricated devices by strong surface pretreatments, three microfabricated device compatible surface cleaning methods have been tested. The methods were selected based on their efficiency in cleaning ambient contamination of gold surfaces as described elsewhere.[28] The investigated methods were: (i) cyclic voltammetry (CV) in 50 mM H_2SO_4 solution, (ii) incubation in dilute basic piranha, i. e. 50 mM KOH and 25% H_2O_2 followed by linear sweep voltammetry in 50 mM KOH and (iii) oxygen plasma treatment followed by incubation in ethanol. The latter method showed lower efficiency in the referenced study[28] but it was attributed to possible contamination of the plasma cleaner, so it was decided to test it in this work. The impact of these pretreatments on the cleanliness and reproducibility of the sensing surfaces has been evaluated. Furthermore, the surface coverage and reproducibility of a model thiolated molecule MCH has been determined. The cleanliness and reproducibility of bare gold surfaces were evaluated by X-ray photoelectron spectroscopy (XPS) and CV. The model probe molecule MCH binding was characterized by CV-mediated reductive desorption and XPS analysis.

MATERIALS AND METHODS

Materials

6-Mercapto-1-hexanol (MCH) ($HS(CH_2)_6OH$, 97%), potassium hydroxide (KOH, 90%), hydrogen peroxide (50 wt.% in H_2O), and potassium chloride (KCl, 99%) were obtained from Sigma (Germany). Sulfuric acid (96%) was purchased from BASF (Sweden). Ethanol (99.5%) was supplied by CCS Healthcare AB (Sweden). SU-8 2002 was obtained from MicroChem (USA). All chemicals were of analytical grade or better and were used as received. All aqueous solutions were prepared in UHQ water with resistivity higher than 18 MΩ × cm.

Methods

Electrode fabrication

Gold electrode chips were fabricated on optically polished PYREX borosilicate glass (Präzisions Glas & Optik, Germany). The 100 nm thickness thermally evaporated Au on 10 nm Ti was patterned by standard UV photolithography and lift-off process. Then SU-8 2002 photoresist was used to define the 0.00785 cm^2 electrode (diameter 1 mm) surface area.

Au pretreatment methods

Dilute basic piranha and linear potential sweep in potassium hydroxide. This pretreatment method has been carried out according to the protocol described previously.[29] Au electrodes were incubated in 50 mM KOH and 25% H_2O_2 for 10 min, and then rinsed with deionized water 5 times. Then, electrode potential was linearly swept from -0.2 V to -1.2 V (vs. Ag/AgCl/saturated KCl) at 50 mV/s scan rate in 50 mM KOH. Afterwards the electrodes were

rinsed with water and dried with N_2. This method has been abbreviated to "KOH + H_2O_2 & LSV".

CV sweep in dilute sulfuric acid. CV sweep in 50 mM sulfuric acid solution is often used for cleaning and evaluating the state of gold electrodes.[30] Au electrodes served as working electrodes and the potential was swept from -0.4 V to 1.4 V (vs. Ag/AgCl/saturated KCl) for 15 cycles at a scan rate of 100 mV/s. After the CV sweep, the electrodes were rinsed with water and dried with N_2. This method has been abbreviated to "CV sweep in H_2SO_4"

Oxygen plasma treatment and ethanol incubation. Au electrodes were cleaned in N_2 and O_2 plasma at 100W for 5 min in a Tepla 300 plasma processor (PVA TePla, Germany). Since plasma treatment can damage the passivating SU-8 layer, the passivating layer thickness was measured before and after the treatment. The plasma treatment parameters were optimized to not alter the passivating layer thickness. Afterwards, the electrodes were incubated in ethanol for 30 min, rinsed with water and dried with N_2. This method has been abbreviated to "O_2 plasma & ethanol".

Electrochemical analysis

Electrochemistry setup. Voltammetric experiments were performed using a VSP 300 (Bio-Logic, France) electrochemical workstation. A conventional 3-electrode cell was used with a laboratory-fabricated polycrystalline gold electrode (see the "Electrode fabrication" section) as the working electrode and a platinum wire (diameter 0.5 mm, ALS Co., Japan) as the counter electrode. All potentials were measured and are quoted against the saturated Ag/AgCl/saturated KCl electrode (ALS Co., Japan). The solutions used in cyclic voltammetry were degassed with N_2 for 30 min prior to each measurement. The temperature was 21°C.

Determination of the electrochemical surface area and roughness factor. Oxygen adsorption measurements were chosen to determine the electrochemical surface area of gold electrodes as described by Trasatti and Petrii.[31] Briefly, a CV measurement was performed in degassed 50 mM H_2SO_4 solution in the potential range from -0.4 V to 1.4 V (vs. Ag/AgCl/saturated KCl) at a scan rate of 100 mV s^{-1}. Then the electrochemical surface area (ESA) was determined as

$$ESA = Q_{AuO} / (400 \mu C \times cm^{-2}), \quad \text{(Eqn. 1)}$$

Q_{AuO} , the reduction charge, was calculated by integrating the cathodic current profile area of the first CV cycle. To avoid errors caused by manual operation, the integrated current profile area was defined by zero current as the baseline and a fixed potential range (0 V to 1.4 V) for all electrodes. A theoretical value for polycrystalline gold of 400 μC × cm^{-2} was used under the assumption that oxygen was chemisorbed on Au in a one-to-one ratio.

The ESA was expressed by roughness factor (R).

$$R = ESA / A_{geo}, \quad \text{(Eqn. 2)}$$

where A_{geo} (0.00785 cm^2) is the geometry of the electrode (diameter 1 mm) area defined by SU-8 passivation.

Determination of MCH surface coverage density (Γ). MCH surface coverage density was evaluated by a method described before.[32] Differently pretreated gold electrodes were immersed in 1 mM MCH aqueous solution for 1 h to form a self-assembled monolayer. Then the electrodes were rinsed with water 5 times and dried with N_2. To determine the MCH surface coverage density (Γ), reductive desorption performed in degassed 100 mM KOH solution by the means of

CV. The potential was swept from 0 V to -1.3 V at a scan rate of 100 mV s^{-1}. The MCH surface coverage density (Γ) was calculated as

$$\Gamma = Q_{re} / (F \times A_{geo}), \quad \text{(Eqn. 3)}$$

where Q_{re} is the charge involved in MCH reductive desorption, F is Faradaic constant, and A_{geo} (0.00785 cm^2) is the geometry of the electrode (diameter 1 mm) area defined by SU-8 passivation. To circumvent the contribution from the charging current, the baseline was set immediately before MCH reductive desorption. In the case of two peaks occurring, both peaks were integrated.

Statistical analysis. The standard deviations between the samples were compared by the F-test. The confidence intervals were evaluated by the t-test (Student's test). The average values and standard deviations were calculated from 5 different samples.

XPS analysis

The XPS characterizations were performed on a Physical Electronics Quantum 2000 Scanning ESCA microprobe with monochromatized Al Kα radiation (hν=1486.7 eV). The background pressure was 6.7×10^{-8} Pa (5×10^{-10} Torr). All spectra were referenced to Au $4f_{7/2}$ (84eV).

XPS analysis of bare Au surfaces. A spot of 100 μm and pass energy of 93.9 eV were used for survey spectra and pass energy of 23.5 eV was used for high-resolution spectra of C1s, O1s. The atomic concentrations were calculated using the sensitivity factor from Casa XPS software.

XPS analysis of MCH modified Au surfaces. A spot of 100 μm and pass energy of 23.5 eV were used for high-resolution spectra of Au 4f and S2p. Data acquisition parameter was kept the

same for all the samples to minimize the differences induced by X-ray radiation caused sample damage.[33] S2p curve fittings were done using Casa XPS software with Shirley background subtraction.

AFM analysis

AFM analysis of bare Au surfaces was performed by a PSIA XE150 Scanning Probe Microscope in a non-contact mode. All images were collected on an area of 1 μm^2 with a resolution of 512 pixels × 512 pixels at a line rate of 0.75 Hz. After the measurements the images were processed with XEI software.

RESULTS AND DISCUSSION

Bare gold electrode characterization

XPS analysis. Survey spectra of microfabricated bare gold electrodes acquired after SU-8 passivation showed marked increases in carbon and oxygen signals indicating contamination. Only trace amounts of other common contaminants, such as nitrogen and chlorine, were found. Since prior to the XPS measurements surfaces before and after SU-8 passivation were exposed to atmosphere at similar conditions, the differences in contamination were mainly caused by SU-8 passivation. Figures 1a and 1b compare the C1s and Au4f peak intensities of the non-passivated (control) surface and SU-8 passivated electrodes before and after different pretreatments.

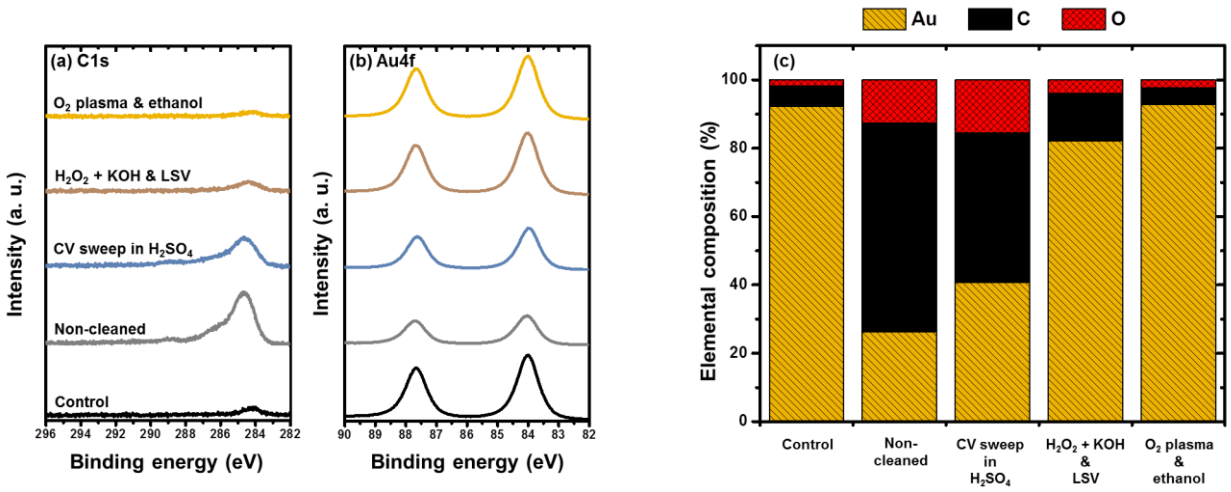

Figure 1. (a) C1s and (b) Au4f spectra and (c) elemental composition of Au electrode (diameter 1 mm) surfaces patterned with SU-8 photolithography before and after pretreatments of "KOH + H_2O_2 & LSV", "CV sweep in H_2SO_4" and "O_2 plasma & ethanol".

The C1s spectrum of the non-cleaned SU-8 passivated gold electrode showed two strong components at approximately 284.8 eV and ~286 eV, and a weak component at ~289 eV, whereas only insignificant quantities of carbon were observed on the non-passivated control surface. The magnitude of the component at 284.8 eV was the highest of the three. The first two peaks were attributed to SU-8 contaminants.[34] The third weak component at ~289 eV corresponded to the C=O bond. While there are no C=O bonds in the SU-8 molecule, they could originate from superficial oxidation during photolithography.

The Au4f spectrum is shown in Figure 1b. The decrease of the Au4f spectrum intensity after SU-8 passivation compares well with the increase of the C1s spectrum intensity. Two peaks of $Au4f_{7/2}$ and $Au4f_{5/2}$ were observed in the gold spectra with the $Au4f_{7/2}$ component registered at 84 eV. The binding energies of the Au4f spectrum reflect the oxidation state of the gold surface. Oxidized gold surfaces exhibit two additional peaks at 85.5 eV and 89.4 eV.[21,35]

These data suggest that gold surfaces were not oxidized before and after pretreatments. It was an important parameter to ensure as oxidized gold surfaces might result in changes in the structural properties of SAMs.[36,37]

As expected, after different gold surface pretreatments significant increases in the intensity of the Au4f spectra with decreases in the C1s spectra intensities were registered. The elemental composition of the differently pretreated surfaces is provided in Figure 1c. After the "O_2 plasma & ethanol" pretreatment, which was the most effective, the surface gold percentage increased 3.5 times and was equal to the value registered on the control surface. In like manner, the carbon percentage decreased 12.5 times and oxygen percentage decreased 5.5 times. The "H_2O_2 + KOH & LSV" pretreatment was the second most efficient method, increasing the gold percentage 3.1 times and decreasing the carbon and oxygen percentages 4.5 and 3.3 times. "CV sweep in H_2SO_4" was the least efficient with the gold percentage increase by 1.6 times and carbon percentage decrease by 1.4 times. The O1s spectra are shown in Figure S1 provided in the Supporting Information.

When comparing the results with those obtained with ambient contaminated gold surfaces[28] the "O_2 plasma & ethanol" pretreatment exhibited the highest efficiency in our study, whereas in the reference the highest changes in elemental composition were obtained after the "H_2O_2 + KOH & LSV" pretreatment. The reported lower efficiency of the plasma treatment in the reference was attributed by the possible contamination of the photoreactor. The efficiency of "CV sweep in H_2SO_4" was also lower for SU-8 contaminated samples as opposed to the ambient contaminated ones.

Electrochemical analysis

In addition to XPS analysis, electrochemical evaluation of the effective surface area and its reproducibility was performed. ESA not only indicates the surface cleanliness but also reveals the relative quantity of sites available for thiol binding. For this reason CV measurements were recorded in 50 mM H_2SO_4 in the potential range between -0.4 V and 1.4 V. The effective surface area was expressed as the roughness factor (R) in this study. In addition, CV measurements at well-defined conditions also provide "fingerprint" information about the chemical and physical state of the gold surface.[38,39]

The integration of the cathodic current profile area defined by the baseline at zero current and the set potential limits was used for the evaluation of R according to the procedure described in the Experimental Section. The voltammograms of differently pretreated samples are shown in Figure 2. The integrated current profile areas are depicted in color.

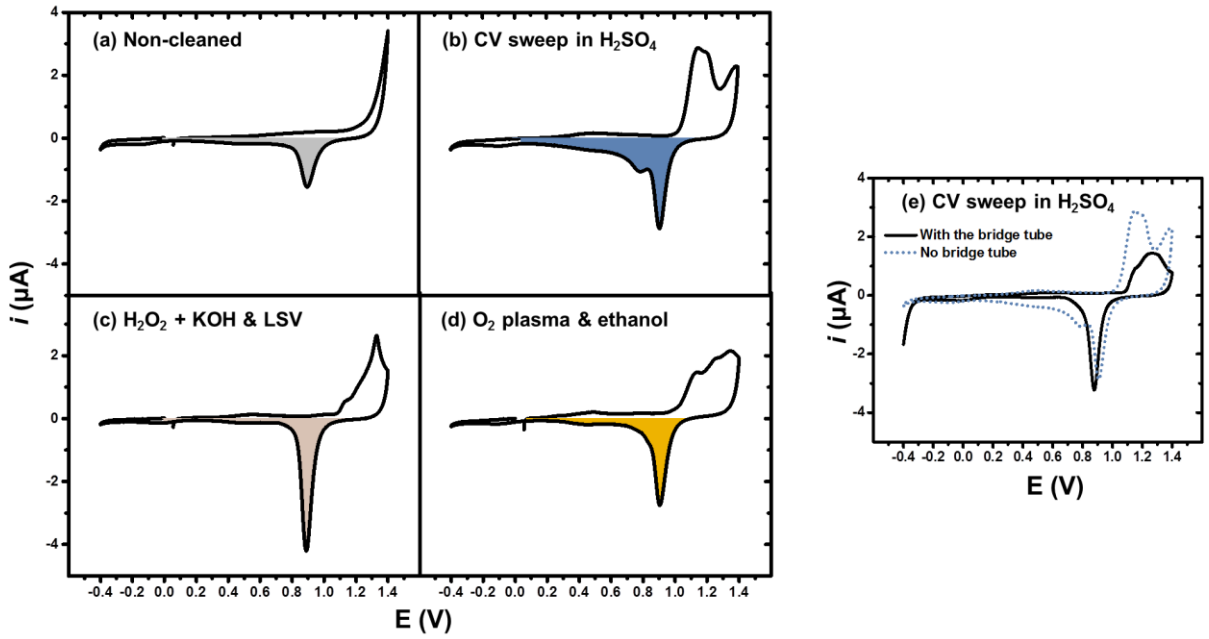

Figure 2. Cyclic voltammograms recorded in 50 mM H_2SO_4 for Au electrodes (diameter 1 mm) patterned with SU-8 photolithography before and after using different pretreatment methods: (a) non-cleaned, (b) after "CV sweep in H_2SO_4", (c) after "H_2O_2 + KOH & LSV" and (d) after "O_2 plasma & ethanol", (e) after "CV sweep in H_2SO_4" with and without the bridge tube. The integrated current profile areas are depicted in color. The scan direction was positive and the scans were initiated at the potential of 0 V vs. Ag/AgCl/saturated KCl.

Problems associated with this method, such as the contribution of the capacitive part of the current, uncertainty which gold oxide is formed and deviations between the assumption of one electron per site exchange and the actual amount of sites determined by defects, were taken into account. Nevertheless, it enabled comparing the investigated pretreatments without the uncertainties of defining the potential limits for separate and overlapping peaks.

In the case of the non-cleaned SU-8 passivated electrode (Figure 2a) no defined features were observed in the double-layer charging region. In the potential range from 1.0 V to 1.4 V gold oxidation could barely be distinguished indicating that contamination strongly decreased the gold atom availability. Consequently, on the return scan the gold oxide reduction peak at ≈0.9 V also exhibited the lowest intensity out of all the investigated samples.

In contrast, after all three pretreatments small peaks were registered at ≈0.5 V. Additionally, the cathodic current in the double-layer charging region was markedly increased after the "CV sweep in H_2SO_4" pretreatment (Figure 2b).

Large increases in the current accounting for the gold oxide formation were observed after all pretreatments. The "H_2O_2 + KOH & LSV" (Figure 2c) and "O_2 plasma & ethanol" (Figure 2d) pretreatments yielded differing oxidation current profiles. Distinct gold oxidation current profile shapes have been discerned to different surface crystallinities.[38] However, despite the current profile differences among the samples and their similarities to those observed on single crystals, it is difficult to conclusively ascertain whether some facets became dominating without further analysis. On the negative sweep, increases in the gold oxide reduction current were observed as well.

After both the "O_2 plasma & ethanol" and "H_2O_2 + KOH & LSV" pretreatments increasing shoulders on the negative side of gold oxide reduction peaks were registered upon continued cycling. The shoulder is only slightly expressed in the first cycles of the "H_2O_2 + KOH & LSV" pretreated sample and absent in the case of "O_2 plasma & ethanol" pretreated sample. As it will be described below, these shoulders stem from dissolved gold redeposition.

Interestingly, electrodes exposed to the "CV sweep in H_2SO_4" pretreatment exhibited a notably different current profile shape from those pretreated by the other two

methods. It had three distinct characteristics. First, current in the gold oxide formation region was markedly elevated and constituted of two overlapping peaks at 1.15 V and 1.2 V. Second, the reduction peak was also split into two: a larger peak at 0.9 V and a smaller one at 0.8 V. Third, a marked increase in the cathodic part of the current was observed in the double-layer charging region below the more negative reduction peak. Peak splitting is not typically observed in polycrystalline gold voltammograms.[39] However, double reduction peaks have been registered in the cases of single-crystal plane gold electrodes with especially developed peak separation in the case of the (110) facet.[38] The appearance of the second reduction peak suggested that the "CV sweep in H_2SO_4" pretreatment might have altered the surface crystallinity ratio of gold or introduced some defects exhibiting similarities to certain gold facets. Thus, it was worthwhile to look into parameters that might have caused the observed results. One potential contributor could be chloride ions leaked from the Ag/AgCl/saturated KCl reference electrode. Chloride induced gold dissolution has been well known in electrochemistry.[40,41] The current profile in Figure 2b was similar to those reported for gold electrodes in chloride containing solutions.[42] In a study of quartz crystal microbalance based evaluation of surface mass changes during potential cycling in the presence of chloride it was concluded that the two merged anodic peaks originate from gold oxidation giving rise to formation of soluble chloride species.[43] Likewise, simultaneous increases in the cathodic current in the double-layer charging region and surface mass were attributed to the redeposition of dissolved species $AuCl_4^-$.

To test this supposition CV measurements using a bridge tube for the reference electrode in order to prevent the chloride leaking were done (Figure 2e). As expected, gold oxidation current was decreased and its current profile shape lost its characteristic shape. Likewise, only one reduction peak was observed on the negative scan. These results proved that

chloride ions were the cause for enhanced gold dissolution followed by its preferential redeposition. What is more, the absence of chloride resulted in the decrease in the current in the double-layer charging region and no peak was observed at ≈0.5 V. Thus, the increased current and peaks in the double-layer charging region was caused by gold oxidation due to chloride adsorption. In accordance, similar peaks in the double-layer charging region were reported in studies on chloride ion adsorption on gold.[44,45] It is also interesting to note that when performing CV measurements with the bridge tube, increasing cathodic current corresponding to hydrogen evolution reaction (HER) was registered in the potential range from -0.3 V to -0.4 V. The most likely explanation for this behavior was platinum dissociation from the counter electrode and deposition on the working electrode, as platinum dissociates in acids during potential cycling.[46] This hypothesis was tested by changing the counter electrode to a graphite rod. In agreement, no HER was registered. In the case of solutions with chloride, a marked decrease in HER may be rationalized as a result of deposition of both gold and platinum ions on the working electrode. This way the surface coverage of platinum on the working electrode would be smaller. Thus, when using the "CV sweep in H_2SO_4" pretreatment it is important to take into account chloride ion leakage from the commonly used reference electrodes, such as Ag/AgCl/saturated KCl or saturated calomel electrode. Chloride induced gold dissolution followed by redeposition yields new surface structures with changed surface characteristics.

Finally, in order to evaluate the gold surface pretreatment reproducibility, R values were calculated according to the procedure described in the Methods part of this paper. The integrated cathodic charge areas are depicted in colors in Figure 2 and the obtained values are provided in Table 1.

Table 1. The reduction charges and roughness factor values obtained from cyclic voltammetry of Au electrodes (diameter 1 mm) patterned with SU-8 lithography before and after using different pretreatments.

Pretreatment	**Reduction charge, C**	**Roughness factor**	**Mean**	**Standard deviation**
Non-cleaned				
	3.09×10^{-6}	0.98	0.93	0.10
	2.57×10^{-6}	0.82		
	3.27×10^{-6}	1.04		
	2.64×10^{-6}	0.84		
	3.06×10^{-6}	0.98		
CV sweep in H_2SO_4				
	4.21×10^{-6}	1.34	1.50	0.14
	5.00×10^{-6}	1.59		
	5.05×10^{-6}	1.61		
	5.09×10^{-6}	1.61		
	4.27×10^{-6}	1.36		
H_2O_2 + KOH & LSV				
	3.83×10^{-6}	1.22	1.34	0.11
	3.92×10^{-6}	1.25		
	4.34×10^{-6}	1.38		
	4.68×10^{-6}	1.49		
	4.33×10^{-6}	1.38		

O_2 plasma & ethanol				
	4.36×10^{-6}	1.39	1.39	0.06
	4.64×10^{-6}	1.48		
	4.15×10^{-6}	1.32		
	4.35×10^{-6}	1.38		
	4.26×10^{-6}	1.36		

Based on the t-test statistically significant differences in the R values were observed when comparing the non-cleaned and differently pretreated electrodes. The increase in the R value was up to 1.5 times in the case of "O_2 plasma & ethanol" pretreated surface. However, no significant differences were observed among the R values obtained after different electrode pretreatments including the "CV sweep in H_2SO_4" pretreatment, which exhibited a distinct current profile shape. Furthermore, the reproducibility values of both non-cleaned surfaces and the pretreated surfaces were not statistically different according to the F-test. Thus, despite the observed differences in cleanliness and surface structure, all three surface pretreatments equally effectively increase R in comparison to the non-cleaned electrodes.

MCH modified gold electrode characterization

After the evaluation of the bare gold electrodes, the effect of surface pretreatment on thiolated molecule binding was evaluated. For this reason, a self-assembled monolayer of MCH was formed on the differently pretreated electrodes. Thiol-terminated molecules adsorb on gold and silver as thiolates.[32,47] Voltammetric reductive desorption of thiols in alkaline solutions proceeds in the following mechanism:

$$X(CH_2)_nS{-}Au + e^- \leftrightarrow X(CH_2)_nS^- + Au \qquad \text{(Eqn. 4)}$$

Assuming that thiolate reductive desorption is a one electron reaction, the surface coverage density can be evaluated by integrating the reductive desorption charge as described in the Methods section. The reductive desorption peak position, its area and shape reflect the adsorption energy, stability, coverage and morphology of the monolayer. Voltammograms of the MCH reductive desorption are shown in Figure 3.

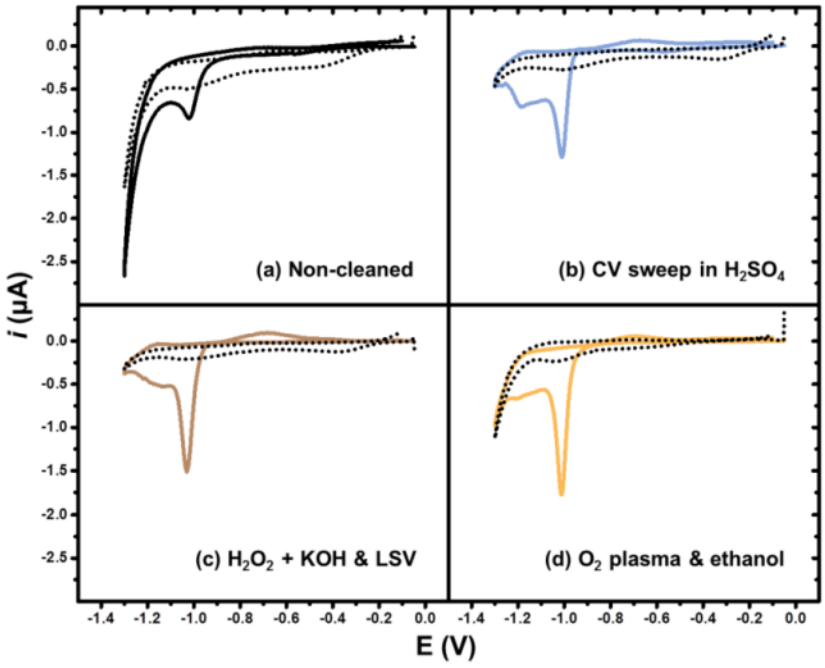

Figure 3. Reductive desorption of MCH (solid line) formed on Au electrodes (diameter 1 mm) patterned with SU-8 photolithography after using different surface pretreatments: (a) non-cleaned, (b) after "CV sweep in H_2SO_4", (c) after "H_2O_2 + KOH & LSV" and (d) after "O_2 plasma & ethanol". The background current is depicted in a dotted line. The electrolyte was 100 mM KOH. The scan direction was negative, the scan rate was 100 mV/s and the scans were initiated at the potential of 0 V vs. Ag/AgCl/saturated KCl.

In the case of the non-cleaned electrode (Figure 3a) on the negative scan one reductive desorption peak was observed in the potential range from -1.01 V to -1.09 V for different samples. Below the peak an increasing cathodic current corresponding to HER or reduction of impurities was registered. On the return scan no clearly defined features were observed.

In contrast, after the electrodes were exposed to different pretreatments the current profiles were changed. First, increases in the MCH reductive desorption peak intensity were observed. The extent of the increase varied slightly for each pretreatment method. The peaks were also narrower than the one registered on the non-cleaned electrode indicating more ordered MCH SAM structures on the pretreated electrodes.[48] Additionally, small broad peaks traceable to oxidative MCH molecule readsorption were observed at -0.8 V on anodic scans after the the investigated surface pretreatments. Finally, significant decreases in current at the negative potential limit were observed after all pretreatments.

However, the most interesting observation is that after all the investigated pretreatments a second, broader peak with a maximum at -1.2 V occurred. The highest intensity of this peak was observed after the "CV sweep in H_2SO_4" pretreatment. A search in the literature revealed that multiple peaks have been observed in some reductive desorption measurements but a consensus on their origin has not been reached.[49]

Different explanations regarding the occurrence of the double peaks have been provided. For instance, it has been suggested that double peaks might originate due to heterogeneity of the SAM layer on the gold surface. On large terraces longer chain thiols (>14 carbon atoms) form a combination of larger and smaller domains. After the cleavage of the gold-thiol bond larger domains do not dissociate from the surface immediately. Instead, they remain as an adlayer in

the double layer region. This way, the more negative peak is believed to originate from the field-induced rearrangement of these molecules.[50,51] Another cause of the two-step reductive desorption could be caused by different SAM molecule resistivities to reductive desorption. It has been suggested that molecules in more compact domains are more resistant to reductive desorption as opposed to those in the less compact ones.[52-54] It has also been proposed that double peaks might arise from different gold-thiol bond strengths of molecules adsorbed on terrace and step sites.[55,56] Similarly, the two reduction peaks might be caused by thiol desorption from different crystalline domains on polycrystalline gold electrodes.[57-59] Furthermore, the more positive peak has also been attributed to the desorption of thiol molecule clusters weakly adsorbed on a densely packed SAM.[60]

Since the majority of explanations above do not to convincingly explain the origin of the Faradaic current observed as the second peak, this uncertainty hampers the understanding and, eventually, control of surface functionalization. It also leads to uncertainties in SAM coverage determination. For instance, if the second peak arises from other phenomena than the reduction of the gold-thiol bond, it should not be included in the thiol surface coverage determination.

To gain further insight into the problem, it is first worth noting that the cases when double peaks are observed generally fall into two categories. In the first instance, the observed potential difference between the peaks is equal or less than 100 mV and in the second, it is more than 100 mV. The first instance is mainly observed in the case of the long chain thiols.[51,61] In our case, however, the difference was ≈200 mV. In order to investigate the origin of the second peak, partial reductive desorption was performed. This way, MCH molecules, which desorb as the first peak, were removed. Then the sample was analyzed by XPS (Figure 4).

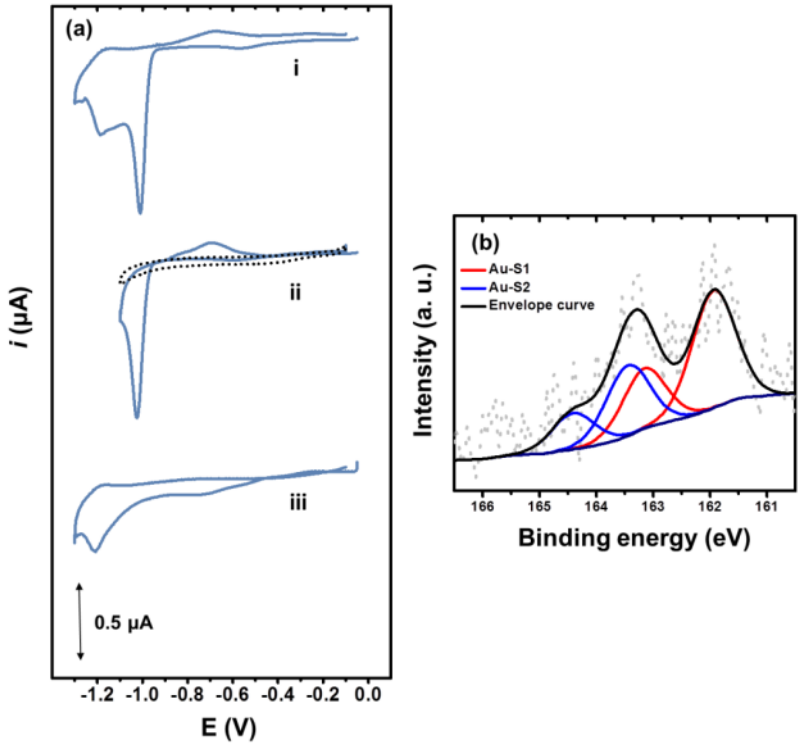

Figure 4. (a) Reductive desorption of MCH formed on Au electrodes (diameter 1 mm) patterned with SU-8 photolithography: (i) full: in the potential range of 0 V – -1.3 V, (ii) partial: in the potential range of 0 V – -1.1 V(1^{st} cycle – solid line; 10^{th} cycle – dashed line) and (iii) desorption in the potential range of 0 V – -1.3 V after partial desorption in the potential range of 0 V – -1.1 V. The scan direction was negative, the scan rate was 100 mV/s and the scans were initiated at the potential of 0 V vs. Ag/AgCl/saturated KCl. (b) S2p spectrum of MCH on Au electrode surface after reductive desorption in the potential range of 0 V – -1.1 V.

Since the second peak was the most expressed in the case of the "CV sweep in H_2SO_4" pretreatment, this method was used for electrode preparation. Figure 4a shows a comparison of reductive desorption voltammograms of full and partial MCH desorption. Case (i) illustrates a voltammogram when MCH reductive desorption is performed in the potential range from 0 V to

-1.3 V. This way, MCH is desorbed in a two-step process yielding two peaks. In the case (ii), the lower potential limit was changed to -1.1 V. By stopping reductive desorption at a higher potential value MCH is only partially desorbed, which results in one reductive desorption peak. As can be seen from the cathodic scan of cycle 1 (blue solid line), as expected, one reductive desorption peak was registered at -1.0 V. On the return scan oxidative MCH readsorption occurred. In order to remove readsorbed molecules CV was run for 10 cycles. In each following cycle readsorbed molecules were desorbed at more positive potentials and lower peak intensities than before (data not shown). More positive reductive desorption potentials suggest that after readsorption MCH molecules form less stable structures. Finally, the inspection of cycle 10 (black dotted line) reveals no desorption or readsorption of the MCH molecules. Thus, MCH was completely removed from the electrode surface in the selected potential range. Eventually, as depicted in the case (iii), the lower potential limit was brought back to -1.3 V. While no peak was observed at -1.0 V, the peak at -1.2 V was registered. It proved that it is possible to isolate the molecules desorbing as the second peak.

To gain more information the sample after partial MCH reductive desorption was subjected to XPS analysis. The S2p spectrum of the sample is shown in Figure 4b. The S2p signal was fitted by two components with $S_{2p3/2}$ peaks at 162 eV and 163.3 eV. The $S_{2p3/2}$ peak at 162 eV is attributed to chemisorbed sulfur atoms. This result was in agreement with the results reported in the literature.[55,62] Thus, it was confirmed that the second peak arises from reductive cleavage of the gold-thiol bond.

As mentioned before, the highest intensity of the second peak was observed after the "CV sweep in H_2SO_4" pretreatment. This pretreatment also yielded the most distinct profile of the bare gold voltammogram indicating alterations in surface gold morphology. Thus, the next step

was investigating whether these two phenomena were related. Several studies of thiols adsorbed on single- and polycrystalline gold substrates demonstrated different reductive desorption peak potentials for different facets. The most positive potential was observed on Au(111), which means that more stable gold-thiol bonds are formed on surfaces with less coordinated gold atoms.[58,59,63] To explore this issue, a non-cleaned gold electrode was pretreated by the "CV sweep in H_2SO_4" for 50 cycles as opposed to the 15 cycles used earlier. The comparison of voltammograms is provided in Figure 5a.

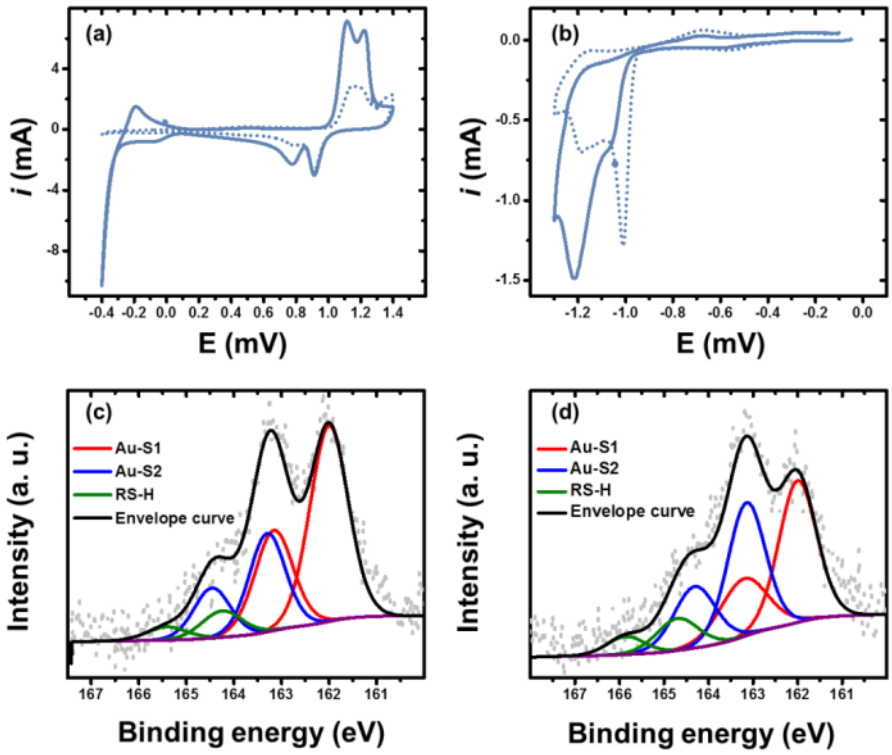

Figure 5. (a) Cyclic voltammograms recorded in 50 mM H_2SO_4 using bare Au electrodes (diameter 1 mm) patterned with SU-8 photolithography and (b) reductive MCH desorption in 100 mM KOH after surface pretreatment by the "CV sweep in H_2SO_4" for 15 (dotted line) and 50

(solid line) cycles. The scan rate was 100 mV/s. XPS S2p spectra of MCH adsorbed on Au electrodes pretreated by "CV sweep in H_2SO_4" for (c) 15 and (d) 50 cycles.

As it can be seen from the figure, after the "CV sweep in H_2SO_4" for 50 cycles the oxidation current was markedly increased and exhibited two well-defined peaks at 1.1 V and 1.2 V. The reduction peak at 0.9 V retained its intensity. However, the intensity of the reduction peak at 0.8 V increased significantly resulting in an altered ratio between these two peaks. These results provided further evidence that chloride induced surface gold atom dissolution and redisposition results in a changed gold facet ratio or introduction of defects. In addition to the CV measurements, atomic force microscopy images were obtained (Figure S2 provided in Supporting Information). These images showed a marked increase in gold grain size, which further supported the hypothesis that the surface was restructured after the "CV sweep in H_2SO_4" for 50 cycles. Although the surface appears to be more uniform due to the larger grain size, the electrochemical behavior of redeposited gold atoms was similar to that for defects and/or of gold facets with gold atoms less coordinated by the lattice.[38] An electrochemical analysis suggests that the fraction of less coordinated gold atoms increased during the pretreatment.

The electrodes pretreated by the "CV sweep in H_2SO_4" for a different number of cycles were then incubated in MCH solutions and subjected to reductive desorption. The voltammograms are provided in Figure 5b. After the "CV sweep in H_2SO_4" for 50 cycles two peaks were observed in both cases. However, in the case of the "CV sweep in H_2SO_4" for 50 cycles the more positive peak was shifted negatively and partially merged with the peak at -1.2 V. It showed a clear relation between the structural state of the surface and molecule binding. The broadened peak shape of the current profile indicated that a less ordered structure was formed. What is more, the

peak intensities were changed dramatically. The intensity of the peak at -1.2 V markedly increased with decreasing intensity of the peak at -1.1 V suggesting the formation of more stable gold-thiol complexes. The results were in accordance with those presented in a study of thiol adsorption on planar and irregular surfaces showing an increased stability of SAMs on surfaces with nanostructure irregularities.[64] These discoveries provide some insights leading to preparation of more stable structures as one of the main disadvantages of SAMs is decomposition with time.[64,65]

With an aim to further investigate these surfaces, the samples were subjected to XPS analysis. The S2p spectra of MCH formed on gold electrodes pretreated by "CV sweep in H_2SO_4" for 15 and 50 cycles are provided in Figures 5c and 5d. The S2p spectra of both samples were fitted to three doublets. A doublet with the $S2p_{3/2}$ peak at 162 eV (shown in red, Au-S1) has been attributed to the bound sulfur. No differences in the binding energy of this doublet between the two samples were observed.

The second doublet (shown in blue, Au-S2) is commonly attributed to unbound sulfur or disulfides. In that case the $S2p_{3/2}$ binding energy should be in the range from 163.5 eV to 164 eV.[62] However, in this study it was 163.2 eV. What is more, the contribution of the $S2p_{3/2}$ component was dominating on electrodes pretreated by "CV sweep in H_2SO_4"for 50 cycles. One explanation could be that these surfaces yielded less ordered SAM structures and consequent interdigitation with the chains of free thiols occurred, as has been observed in the case of longer chain thiols.[66] To test this possibility reductive desorption measurements of MCH SAMs formed from micromolar solutions were done. This minimized the possibility of multilayer formation. However, multiple peaks were still observed in voltammograms (data not shown). In addition to the experimental results, there are more arguments against interdigitation. First, interdigitation

has been observed on long chain alkanethiols due to chain-chain interactions. It less likely to occur with short chain, water soluble thiols, such as the MCH used in this study. Moreover, the samples were thoroughly rinsed after the modification with MCH. Finally, the intensity of the $S2p_{3/2}$ peak at 163.3 eV correlated with the intensity of the MCH reductive desorption peak at -1.1 V suggesting that it stemmed from the formation of more stable gold-thiol complexes. For these reasons, it was not likely that an increase in $S2p_{3/2}$ component was caused by the unbound molecules. Another explanation could be based on an observation of a similar $S_{2p3/2}$ peak at 163.2 eV – 163.3 eV in a study of thiol self-assembly on different gold single crystals.[33] The peak was attributed to the X-ray induced MCH molecule damage. It could be that due to different morphologies of the electrodes MCH monolayers exhibited different sensitivities to the X-rays. However, the peak at 163.2 eV probably originates from another species of gold-thiol bond. It has been shown, for instance, that XPS spectra of methanethiol molecules adsorbed on Cu(111) and Au(111) yield several components with different binding energies (having a peak at 163.5 eV in the case of methanethiol on gold) when the metal surfaces are exposed to higher temperatures causing surface reconstruction. These binding energies have been attributed to methanethiol binding on different surface sites, such as top, bridging and hollow sites[67,68] although it has also been suggested that the differences between the forms of sulfur binding to step and terrace sites should be about 0.2 eV-0.3 eV.[55] Interestingly, a new model supplementing the current understanding of gold-thiolate bonds has been recently accepted.[69] In addition to the usual monothiolate binding to the different sites of the gold surface, other binding configurations have been revealed, for instance, disulfide bonding, thiolate binding to the adatoms and adatom bridging by monothiolates.[69] Such variations in gold-thiolate bonds could explain the correlation

between the changed surface structure after the "CV sweep in H_2SO_4" pretreatment, reductive desorption and photoemission spectra.

The last doublet (shown in green, R-SH) with the $S2p_{3/2}$ component at 164.3 eV for the 15 cycles swept electrode and at 164.7 eV for the 50 cycles swept electrode was attributed to the unbound sulfur species.[62]

Since it was determined that the second peak observed in the reductive desorption measurements arises from the gold-thiolate bonds, the areas of both peaks were integrated in order to calculate the MCH surface coverage and their reproducibility before and after the investigated pretreatments. Even with the roughness factor taken into account the obtained surface coverage values were from 1.41 to 2.47 times larger than the theoretical surface coverage value of $\Gamma=8 \times 10^{-10}$ mol cm^{-2} for a thiol monolayer adsorbed on Au(111) surface.[32] This difference could be attributed to the uncertainties of the method, such as difficulties in defining peak limits, influence of the capacitive current and, in some cases, overlapping HER current, in addition to the uncertainties in determination of the surface roughness factor. Thus, the MCH surface coverages were not derived entirely from the Faradaic charge of the gold-thiol bond cleavage. However, since the main aim of this evaluation was to compare different pretreatments and their reproducibility, the method was still deemed to be fit to achieve the desired results. The MCH reductive desorption charges and the calculated surface coverages before and after different pretreatments are provided in Table 2.

Table 2. The MCH reductive desorption charge and surface coverage values obtained from cyclic voltammetry using differently pretreated Au electrodes (diameter 1 mm) patterned with SU-8 photolithography.

Pretreatment	**Q,** **C × cm^{-2}**	**Γ,** **mol × cm^{-2}**	**Γ_{mean},** **mol × cm^{-2}**	**Standard deviation**
Non-cleaned				
	9.67×10^{-5}	1.00×10^{-9}	1.05×10^{-9}	6.92×10^{-11}
	9.53×10^{-5}	9.87×10^{-10}		
	7.92×10^{-4}	1.05×10^{-9}		
	8.80×10^{-4}	1.16×10^{-9}		
	8.09×10^{-4}	1.07×10^{-9}		
CV sweep in H_2SO_4				
	1.25×10^{-4}	1.30×10^{-9}	2.09×10^{-9}	4.58×10^{-10}
	2.18×10^{-4}	2.26×10^{-9}		
	2.25×10^{-4}	2.33×10^{-9}		
	2.06×10^{-4}	2.14×10^{-9}		
	2.35×10^{-4}	2.44×10^{-9}		
H_2O_2 + KOH & LSV				
	1.77×10^{-4}	1.83×10^{-9}	2.19×10^{-9}	2.05×10^{-10}
	2.23×10^{-4}	2.31×10^{-9}		
	2.20×10^{-4}	2.28×10^{-9}		
	2.13×10^{-4}	2.21×10^{-9}		
	2.24×10^{-4}	2.32×10^{-9}		

O_2 plasma & ethanol				
	2.06×10^{-4}	2.14×10^{-9}	2.75×10^{-9}	3.95×10^{-10}
	2.92×10^{-4}	3.02×10^{-9}		
	2.53×10^{-4}	2.62×10^{-9}		
	3.05×10^{-4}	3.16×10^{-9}		
	2.68×10^{-4}	2.78×10^{-9}		

Similarly to the case of the bare gold electrodes, the differences in MCH surface coverages were statistically significant before and after different pretreatments based on t-test analysis. The average MCH surface coverage was up to 2.75 times higher in the case of "O_2 plasma & ethanol" pretreatment. However, when comparing different pretreatment methods, no significant differences in reproducibility among them have been observed.

CONCLUSIONS

A comprehensive and systematic evaluation of the preparation of microfabricated gold sensor surfaces aimed at biosensing has been presented. Based on CV and XPS analysis it was shown that photoresist SU-8 mediated photolithography causes marked contamination of the gold surface, which results in strongly decreased surface area and, consequently, significantly lower surface functionalization efficiency. In turn, it has also been demonstrated that the contamination can be significantly reduced and the molecule surface coverage can be improved by microfabricated device compatible gold surface pretreatments, more specifically, (i) cyclic voltammetry in dilute H_2SO_4, (ii) dilute basic piranha followed by LSV in dilute KOH and (iii)

O_2 plasma treatment followed by incubation in ethanol. No significant differences in ESA or MCH coverage were observed after different electrode pretreatments. The ESA could be improved by up to 1.5 times and MCH coverage – up to 2.75 times respectively.

However, most importantly the study provided insights on the significance of understanding and accounting for the effects on the sensing surface induced by the pretreatment methods. It has been revealed that different pretreatments, especially the ones involving chloride, induce structural gold surface changes resulting in redistribution of the gold surface and/or introduction of surface defects. In addition to that, it has also been shown that surface alterations influence morphological structure of the thiolated molecule layer. The findings presented in this paper will help to better understand and control microfabricated biosensor surface preparation, which is critical for their successful implementation and commercialization. Furthermore, the presented knowledge can be extended to other biosensor types that also employ gold surfaces. A comprehensive understanding of biosensor surface preparation will contribute to optimization of biosensor surfaces and full exploitation of their potential.

ACKNOWLEDGEMENTS

This work was supported by the Swedish Strategic Research Foundation (SSF ICA 12-0047 and FFL15-0174), the Swedish Research Council (VR 2014-5588), Carl Tryggers Foundation (CTS14-527), and the Wallenberg Academy Fellow Program. The authors would also like to thank Dr Patrik Ahlberg for contributing to the Abstract Graphic.

REFERENCES

(1) Nayak, S.; Blumenfeld, N. R.; Laksanasopin, T.; Sia, S. K. Point-of-Care Diagnostics: Recent Developments in a Connected Age. *Anal. Chem.* **2017**, *89* (1), 102–123.

(2) Rotariu, L.; Lagarde, F.; Jaffrezic-Renault, N.; Bala, C. Electrochemical Biosensors for Fast Detection of Food Contaminants – Trends and Perspective. *TrAC Trends Anal. Chem.* **2016**, *79*, 80–87.

(3) Sergeev, N. V.; Herold, K. E.; Rasooly, A. Regulatory and Validation Issues for Biosensors and Related Bioanalytical Technologies. In *Handbook of Biosensors and Biochips*; John Wiley & Sons, Ltd, 2008.

(4) Qing, Q.; Jiang, Z.; Xu, L.; Gao, R.; Mai, L.; Lieber, C. M. Free-Standing Kinked Nanowire Transistor Probes for Targeted Intracellular Recording in Three Dimensions. *Nat. Nanotechnol.* **2014**, *9* (2), 142–147.

(5) Duan, X.; Li, Y.; Rajan, N. K.; Routenberg, D. A.; Modis, Y.; Reed, M. A. Quantification of the Affinities and Kinetics of Protein Interactions Using Silicon Nanowire Biosensors. *Nat. Nanotechnol.* **2012**, *7* (6), 401–407.

(6) Ingebrandt, S.; Han, Y.; Nakamura, F.; Poghossian, A.; Schöning, M. J.; Offenhäusser, A. Label-Free Detection of Single Nucleotide Polymorphisms Utilizing the Differential Transfer Function of Field-Effect Transistors. *Biosens. Bioelectron.* **2007**, *22* (12), 2834–2840.

(7) Rothberg, J. M.; Hinz, W.; Rearick, T. M.; Schultz, J.; Mileski, W.; Davey, M.; Leamon, J. H.; Johnson, K.; Milgrew, M. J.; Edwards, M.; Hoon, J.; Simons, J. F.; Marran, D.; Myers, J. W.; Davidson, J. F.; Branting, A.; Nobile, J. R.; Puc, B. P.; Light, D.; Clark, T. A.; Huber, M.; Branciforte, J. T.; Stoner, I. B.; Cawley, S. E.; Lyons, M.; Fu, Y.; Homer, N.; Sedova, M.; Miao, X.; Reed, B.; Sabina, J.; Feierstein, E.; Schorn, M.; Alanjary, M.; Dimalanta, E.; Dressman, D.; Kasinskas, R.; Sokolsky, T.; Fidanza, J. A.; Namsaraev, E.; McKernan, K. J.; Williams, A.; Roth, G. T.; Bustillo, J. An Integrated Semiconductor Device Enabling Non-Optical Genome Sequencing. *Nature* **2011**, *475* (7356), 348–352.

(8) Mohanty, S. P.; Kougianos, E. Biosensors: A Tutorial Review. *IEEE Potentials* **2006**, *25* (2), 35–40.

(9) Estrela, P.; Stewart, A.G., Yan, F., Migliorato, P. Field Effect Detection of Biomolecular Interactions. *Electrochim. Acta* **2005**, *50* (25-26), 4995–5000.

(10) Yan, F., Mok, S. M., Yu, J., Chan, H. L. W., Yang, M. Label-Free DNA Sensor Based on Organic Thin Film Transistors. *Biosens. Bioelectron.* **2009**, *24* (5), 1241–1245.

(11) Kimura-Suda, H., Petrovykh, D. Y., Tarlov, M. J., Whitman, L. J. Base-Dependent Competitive Adsorption of Single-Stranded DNA on Gold. *J. Am. Chem. Soc.* **2003** *125* (30), 9014–9015.

(12) Petrovykh, D. Y., Kimura-Suda, H., Whitman, L. J., Tarlov, M. J. Quantitative Analysis and Characterization of DNA Immobilized on Gold. *J. Am. Chem. Soc.* **2003**, *125* (17), 5219–5226.

(13) Levicky, R., Herne, T. M., Tarlov., M. J., Satija, S. K. Using Self-Assembly To Control the Structure of DNA Monolayers on Gold: A Neutron Reflectivity Study. *J. Am. Chem. Soc.* **1998**, *120* (38), 9787–9792.

(14) Lao, R., Song, S., Wu, H., Wang, L., Zhang, Z., He, L., Fan, C. Electrochemical Interrogation of DNA Monolayers on Gold Surfaces. *Analytical Chemistry* **2005,** *77* (19), 6475–6480.

(15) Herne, T. M.; Tarlov, M. J. Characterization of DNA Probes Immobilized on Gold Surfaces. *J. Am. Chem. Soc.* **1997**, *119* (38), 8916–8920.

(16) Arinaga, K.; Rant, U.; Tornow, M.; Fujita, S.; Abstreiter, G.; Yokoyama, N. The Role of Surface Charging during the Coadsorption of Mercaptohexanol to DNA Layers on Gold: Direct Observation of Desorption and Layer Reorientation. *Langmuir* **2006**, *22* (13), 5560–5562.
(17) Wong, E. L. S., Chow, E., Gooding, J. J., DNA Recognition Interfaces: The Influence of Interfacial Design on the Efficiency and Kinetics of Hybridization. *Langmuir* **2005** *21* (15), 6957–6965.
(18) Bubendorfer, A. J.; Ingham, B.; Kennedy, J. V.; Arnold, W. M. Contamination of PDMS Microchannels by Lithographic Molds. *Lab Chip* **2013**, *13* (22), 4312–4316.
(19) Macintyre, D. S.; Ignatova, O.; Thoms, S.; Thayne, I. G. Resist Residues and Transistor Gate Fabrication. *J. Vac. Sci. Technol. B Microelectron. Nanometer Struct. Process. Meas. Phenom.* **2009**, *27* (6), 2597–2601.
(20) Thomas, J. P.; Zhao, L.; Ding, K.; Heinig, N. F.; Leung, K. T. Near-Surface Oxidized Sulfur Modifications and Self-Assembly of Thiol-Modified Aptamer on Au Thin Film Substrates Influenced by Piranha Treatment. *ACS Appl. Mater. Interfaces* **2012**, *4* (11), 5945–5948.
(21) Koslowski, B.; Boyen, H.-G.; Wilderotter, C.; Kästle, G.; Ziemann, P.; Wahrenberg, R.; Oelhafen, P. Oxidation of Preferentially (1 1 1)-Oriented Au Films in an Oxygen Plasma Investigated by Scanning Tunneling Microscopy and Photoelectron Spectroscopy. *Surf. Sci.* **2001**, *475* (1–3), 1–10.
(22) Murphy, J. N.; Cheng, A. K. H.; Yu, H.-Z.; Bizzotto, D. On the Nature of DNA Self-Assembled Monolayers on Au: Measuring Surface Heterogeneity with Electrochemical in Situ Fluorescence Microscopy. *J. Am. Chem. Soc.* **2009**, *131* (11), 4042–4050.
(23) Zhang, D.; Must, I.; Netzer, N. L.; Xu, X.; Solomon, P.; Zhang, S.-L.; Zhang, Z. Direct Assessment of Solid–Liquid Interface Noise in Ion Sensing Using a Differential Method. *Appl. Phys. Lett.* **2016**, *108* (15), 151603.
(24) Martinoia, S.; Rosso, N.; Grattarola, M.; Lorenzelli, L.; Margesin, B.; Zen, M. Development of ISFET Array-Based Microsystems for Bioelectrochemical Measurements of Cell Populations. *Biosens. Bioelectron.* **2001**, *16* (9–12), 1043–1050.
(25) Lorenz, H.; Despont, M.; Fahrni, N.; LaBianca, N.; Renaud, P.; Vettiger, P. SU-8: A Low-Cost Negative Resist for MEMS. *J. Micromechanics Microengineering* **1997**, *7* (3), 121–124.
(26) Abgrall, P.; Conedera, V.; Camon, H.; Gue, A.-M.; Nguyen, N.-T. SU-8 as a Structural Material for Labs-on-Chips and Microelectromechanical Systems. *Electrophoresis* **2007**, *28* (24), 4539–4551.
(27) Dai, W.; Lian, K.; Wang, W. A Quantitative Study on the Adhesion Property of Cured SU-8 on Various Metallic Surfaces. *Microsyst. Technol.* **2005**, *11* (7), 526–534.
(28) Fischer, L. M.; Tenje, M.; Heiskanen, A. R.; Masuda, N.; Castillo, J.; Bentien, A.; Émneus, J.; Jakobsen, M. H.; Boisen, A. Gold Cleaning Methods for Electrochemical Detection Applications. *Microelectron. Eng.* **2009**, *86* (4–6), 1282–1285.
(29) Heiskanen, A. R.; Spégel, C. F.; Kostesha, N.; Ruzgas, T.; Emnéus, J. Monitoring of Saccharomyces Cerevisiae Cell Proliferation on Thiol-Modified Planar Gold Microelectrodes Using Impedance Spectroscopy. *Langmuir* **2008**, *24* (16), 9066–9073.
(30) Spégel, C.; Heiskanen, A.; Acklid, J.; Wolff, A.; Taboryski, R.; Emnéus, J.; Ruzgas, T. On-Chip Determination of Dopamine Exocytosis Using Mercaptopropionic Acid Modified Microelectrodes. *Electroanalysis* **2007**, *19* (2–3), 263–271.
(31) Trasatti, S.; Petrii, O. A. Real Surface Area Measurements in Electrochemistry. *Pure Appl. Chem.* **2009**, *63* (5), 711–734.

(32) Walczak, M. M.; Popenoe, D. D.; Deinhammer, R. S.; Lamp, B. D.; Chung, C.; Porter, M. D. Reductive Desorption of Alkanethiolate Monolayers at Gold: A Measure of Surface Coverage. *Langmuir* **1991**, *7* (11), 2687–2693.
(33) Laiho, T.; Leiro, J. A.; Lukkari, J. XPS Study of Irradiation Damage and Different Metal–sulfur Bonds in Dodecanethiol Monolayers on Gold and Platinum Surfaces. *Appl. Surf. Sci.* **2003**, *212–213*, 525–529.
(34) Walther, F.; Davydovskaya, P.; Zürcher, S.; Kaiser, M.; Herberg, H.; Gigler, A. M.; Stark, R. W. Stability of the Hydrophilic Behavior of Oxygen Plasma Activated SU-8. *J. Micromechanics Microengineering* **2007**, *17* (3), 524.
(35) Tsai, H.; Hu, E.; Perng, K.; Chen, M.; Wu, J.-C.; Chang, Y.-S. Instability of Gold Oxide Au_2O_3. *Surf. Sci.* **2003**, *537* (1–3), 447–450.
(36) Ron, H.; Rubinstein, I. Alkanethiol Monolayers on Preoxidized Gold. Encapsulation of Gold Oxide under an Organic Monolayer. *Langmuir* **1994**, *10* (12), 4566–4573.
(37) Woodward, J. T.; Walker, M. L.; Meuse, C. W.; Vanderah, D. J.; Poirier, G. E.; Plant, A. L. Effect of an Oxidized Gold Substrate on Alkanethiol Self-Assembly. *Langmuir* **2000**, *16* (12), 5347–5353.
(38) Hamelin, A. Cyclic Voltammetry at Gold Single-Crystal Surfaces. Part 1. Behaviour at Low-Index Faces. *J. Electroanal. Chem.* **1996**, *407* (1), 1–11.
(39) Declan Burke, L., O'Mullane, A. Generation of Active Surface States of Gold and the Role of Such States in Electrocatalysis. .J. Solid State Electrochem. **2000**, 4 (5), 285–297.
(40) Wiechers, J.; Twomey, T.; Kolb, D. M.; Behm, R. J. An in-Situ Scanning Tunneling Microscopy Study of Au (111) with Atomic Scale Resolution. *J. Electroanal. Chem. Interfacial Electrochem.* **1988**, *248* (2), 451–460.
(41) Trevor, D. J.; Chidsey, C. E. D.; Loiacono, D. N. In Situ Scanning-Tunneling-Microscope Observation of Roughening, Annealing, and Dissolution of Gold (111) in an Electrochemical Cell. *Phys. Rev. Lett.* **1989**, *62* (8), 929–932.
(42) Ye, S.; Ishibashi, C.; Uosaki, K. Anisotropic Dissolution of an Au(111) Electrode in Perchloric Acid Solution Containing Chloride Anion Investigated by in Situ STM – The Important Role of Adsorbed Chloride Anion. *Langmuir* **1999**, *15* (3), 807–812.
(43) Ye, S.; Ishibashi, C.; Shimazu, K.; Uosaki, K. An In Situ Electrochemical Quartz Crystal Microbalance Study of the Dissolution Process of a Gold Electrode in Perchloric Acid Solution Containing Chloride Ion. *J. Electrochem. Soc.* **1998**, *145* (5), 1614–1623.
(44) Melendres, C. A.; Hahn, F. "In-Situ" Observation of Halide Ion Adsorption on a Gold Electrode Using Synchrotron Far Infrared Spectroscopy. *J. Electroanal. Chem.* **1999**, *463* (2), 258–261.
(45) Bozzini, B.; Cerullo, G.; D'Urzo, L.; Polli, D. In Situ Femtosecond Spectroelectrochemistry of Au(1 1 1) in an Aqueous Chloride Solution. *Electrochem. Commun.* **2009**, *11* (4), 799–803.
(46) Topalov, A. A.; Cherevko, S.; Zeradjanin, A. R.; Meier, J. C.; Katsounaros, I.; Mayrhofer, K. J. J. Towards a Comprehensive Understanding of Platinum Dissolution in Acidic Media. *Chem. Sci.* **2013**, *5* (2), 631–638.
(47) Widrig, C. A.; Chung, C.; Porter, M. D. The Electrochemical Desorption of N-Alkanethiol Monolayers from Polycrystalline Au and Ag Electrodes. *J. Electroanal. Chem. Interfacial Electrochem.* **1991**, *310* (1), 335–359.

(48) Kakiuchi, T., Usui, H., Hobara, D., Yamamoto, M. Voltammetric Properties of the Reductive Desorption of Alkanethiol Self-Assembled Monolayers from a Metal Surface. *Langmuir* **2002** *18* (13), 5231–5238.
(49) Feng, G.; Niu, T.; You, X.; Wan, Z.; Kong, Q.; Bi, S. Studies on the Effect of Electrode Pretreatment on the Coverage of Self-Assembled Monolayers of Dodecanethiol on Gold by Electrochemical Reductive Desorption Determination. *Analyst* **2011**, *136* (23), 5058–5063.
(50) Byloos, M.; Al-Maznai, H.; Morin, M. Formation of a Self-Assembled Monolayer via the Electrospreading of Physisorbed Micelles of Thiolates. *J. Phys. Chem. B* **1999**, *103* (31), 6554–6561.
(51) Wong, S.-S.; Porter, M. D. Origin of the Multiple Voltammetric Desorption Waves of Long-Chain Alkanethiolate Monolayers Chemisorbed on Annealed Gold Electrodes. *J. Electroanal. Chem.* **2000**, *485* (2), 135–143.
(52) Zhong, C.-J.; Porter, M. D. Fine Structure in the Voltammetric Desorption Curves of Alkanethiolate Monolayers Chemisorbed at Gold. *J. Electroanal. Chem.* **1997**, *425* (1–2), 147–153.
(53) Yang, D.-F.; Wilde, C. P.; Morin, M. Studies of the Electrochemical Removal and Efficient Re-Formation of a Monolayer of Hexadecanethiol Self-Assembled at an Au(111) Single Crystal in Aqueous Solutions. *Langmuir* **1997**, *13* (2), 243–249.
(54) Kim, M.; Hohman, J. N.; Serino, A. C.; Weiss, P. S. Structural Manipulation of Hydrogen-Bonding Networks in Amide-Containing Alkanethiolate Monolayers via Electrochemical Processing. *J. Phys. Chem. C* **2010**, *114* (46), 19744–19751.
(55) Walczak, M. M.; Alves, C. A.; Lamp, B. D.; Porter, M. D. Electrochemical and X-Ray Photoelectron Spectroscopic Evidence for Differences in the Binding Sites of Alkanethiolate Monolayers Chemisorbed at Gold. *J. Electroanal. Chem.* **1995**, *396* (1–2), 103–114.
(56) Vericat, C.; Andreasen, G.; Vela, M. E.; Martin, H.; Salvarezza, R. C. Following Transformation in Self-Assembled Alkanethiol Monolayers on Au(111) by in Situ Scanning Tunneling Microscopy. *J. Chem. Phys.* **2001**, *115* (14), 6672–6678.
(57) Yang, D.-F.; Wilde, C. P.; Morin, M. Electrochemical Desorption and Adsorption of Nonyl Mercaptan at Gold Single Crystal Electrode Surfaces. *Langmuir* **1996**, *12* (26), 6570–6577.
(58) Arihara, K.; Ariga, T.; Takashima, N.; Arihara, K.; Okajima, T.; Kitamura, F.; Tokuda, K.; Ohsaka, T. Multiple Voltammetric Waves for Reductive Desorption of Cysteine and 4-Mercaptobenzoic Acid Monolayers Self-Assembled on Gold Substrates. *Phys. Chem. Chem. Phys.* **2003**, *5* (17), 3758–3761.
(59) Doneux, T.; Steichen, M.; De Rache, A.; Buess-Herman, C. Influence of the Crystallographic Orientation on the Reductive Desorption of Self-Assembled Monolayers on Gold Electrodes. *J. Electroanal. Chem.* **2010**, *649* (1–2), 164–170.
(60) Carvalhal, R. F.; Freire, R. S.; Kubota, L. T. Polycrystalline Gold Electrodes: A Comparative Study of Pretreatment Procedures Used for Cleaning and Thiol Self-Assembly Monolayer Formation. *Electroanalysis* **2005**, *17* (14), 1251–1259.
(61) Thom, I.; Buck, M. Electrochemical Stability of Self-Assembled Monolayers of Biphenyl Based Thiols Studied by Cyclic Voltammetry and Second Harmonic Generation. *Surf. Sci.* **2005**, *581* (1), 33–46.

(62) Castner, D. G.; Hinds, K.; Grainger, D. W. X-Ray Photoelectron Spectroscopy Sulfur 2p Study of Organic Thiol and Disulfide Binding Interactions with Gold Surfaces. *Langmuir* **1996**, *12* (21), 5083–5086.
(63) Madueño, R.; Sevilla, J. M.; Pineda, T.; Román, A. J.; Blázquez, M. A Voltammetric Study of 6-Mercaptopurine Monolayers on Polycrystalline Gold Electrodes. *J. Electroanal. Chem.* **2001**, *506* (2), 92–98.
(64) Vericat, C.; Benitez, G. A.; Grumelli, D. E.; Vela, M. E.; Salvarezza, R. C. Thiol-Capped Gold: From Planar to Irregular Surfaces. *J. Phys. Condens. Matter* **2008**, *20* (18), 184004.
(65) Wirde, M.; Gelius, U.; Nyholm, L. Self-Assembled Monolayers of Cystamine and Cysteamine on Gold Studied by XPS and Voltammetry. *Langmuir* **1999**, *15* (19), 6370–6378.
(66) Pradeep, T.; Sandhyarani, N. Structure and Dynamics of Monolayers on Planar and Cluster Surfaces. *Pure Appl. Chem.* **2009**, *74* (9), 1593–1607.
(67) Liu, G.; Rodriguez, J. A.; Dvorak, J.; Hrbek, J.; Jirsak, T. Chemistry of Sulfur-Containing Molecules on Au(1 1 1): Thiophene, Sulfur Dioxide, and Methanethiol Adsorption. *Surf. Sci.* **2002**, *505*, 295–307.
(68) Jackson, G. J.; Woodruff, D. P.; Jones, R. G.; Singh, N. K.; Chan, A. S. Y.; Cowie, B. C. C.; Formoso, V. Following Local Adsorption Sites through a Surface Chemical Reaction: CH_3SH on Cu(111). *Phys. Rev. Lett.* **2000**, *84* (1), 119–122.
(69) Häkkinen, H. The Gold-Sulfur Interface at the Nanoscale. *Nat. Chem.* **2012**, *4* (6), 443–455.

ABSTRACT GRAPHIC

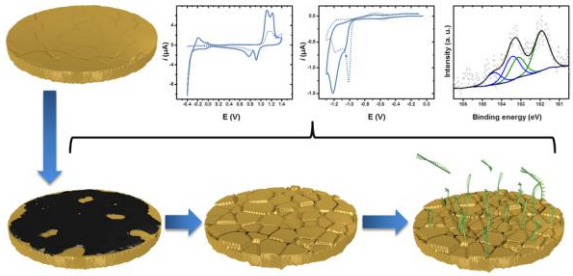

Supporting Information. The file includes O1s spectra of Au electrode surfaces before and after pretreatment by different cleaning methods and AFM images of surfaces before and after "CV sweep in in H_2SO_4" pretreatment for 15 cycles and 50 cycles.